Orientation of the N-Terminal Lobe of the Myosin Regulatory Light Chain in Skeletal Muscle Fibers

Daniela Romano,[†] Birgit D. Brandmeier,[†‡] Yin-Biao Sun,[‡] David R. Trentham,[†] and Malcolm Irving[‡*]
[†]Medical Research Council, National Institute for Medical Research, London, United Kingdom; and [‡]Randall Division of Cell and Molecular Biophysics, King's College London, London, United Kingdom

ABSTRACT The orientation of the N-terminal lobe of the myosin regulatory light chain (RLC) in demembranated fibers of rabbit psoas muscle was determined by polarized fluorescence. The native RLC was replaced by a smooth muscle RLC with a bifunctional rhodamine probe attached to its A, B, C, or D helix. Fiber fluorescence data were interpreted using the crystal structure of the head domain of chicken skeletal myosin in the nucleotide-free state. The peak angle between the lever axis of the myosin head and the fiber or actin filament axis was 100—110° in relaxation, isometric contraction, and rigor. In each state the hook helix was at an angle of ~40° to the lever/filament plane. The in situ orientation of the RLC D and E helices, and by implication of its N- and C-lobes, was similar in smooth and skeletal RLC isoforms. The angle between these two RLC lobes in rigor fibers was different from that in the crystal structure. These results extend previous crystallographic evidence for bending between the two lobes of the RLC to actin-attached myosin heads in muscle fibers, and suggest that such bending may have functional significance in contraction and regulation of vertebrate striated muscle.

INTRODUCTION

Muscle contraction is driven by a structural change or working stroke in the head domain of a myosin molecule, coupled to ATP hydrolysis (1–3). A major component of the working stroke is associated with rotation of the light chain binding or lever arm domain (LCD) of the myosin head with respect to its actin-bound catalytic domain (4–6). This lever arm model, at least in its simplest form, implies that the LCD is relatively rigid, so that its rotation with respect to the catalytic domain is transferred efficiently to its connection with the myosin filament. However, crystallographic studies of isolated myosin head fragments have provided evidence for flexibility within the LCD (7–10). In smooth muscle and invertebrate skeletal muscle, changes in LCD conformation associated with internal flexibility are likely to be linked to myosin-based regulation of contraction (11). The functional significance of LCD flexibility in vertebrate striated muscle is less clear. X-ray and fluorescence studies have shown that rotation of the LCD is associated with the internal elasticity of the myosin head as well as with the working stroke (12,13), but did not establish the location of the elastic element within the myosin head.

We have been investigating LCD conformation in skeletal muscle fibers using bifunctional rhodamine (BR) probes attached to specific pairs of amino acid side chains on the surface of the myosin regulatory and essential light chains (14–17). We have expressed mutant light chains in which the selected residues were replaced by cysteines; we cross-linked each cysteine pair with BR, exchanged the pure labeled light chains into isolated demembranated fibers from skeletal muscle, and determined the orientation of the BR inside the fiber by polarized fluorescence. Earlier studies of this type (14–16) targeted the C-terminal lobe of the myosin regulatory light chain (RLC) from smooth muscle (smRLC), which can replace the native RLC of skeletal muscle myosin (skRLC) without loss of muscle fiber function, and can also be used in a myofibrillar ATPase assay for RLC function (18–20). A subsequent study (17) used the BR probe at three different sites on the N-terminal lobe of the essential light chain of skeletal muscle myosin (skELC), and showed that one of the points of flexibility in the LCD suggested by crystallography, between its ELC and RLC regions, was present in actin-attached myosin heads in vertebrate skeletal muscle fibers.

Here, we extend the approach to the N-terminal lobe of the RLC (Fig. 1), which wraps around the C-terminal hook helix of the myosin head domain, in a location where it could control the bend between the hook helix and the adjacent long helix that forms the backbone of the lever arm. A recent crystallographic study of the LCD of a myosin from the catch muscle of the scallop *Placopecten magellanicus* (9) revealed structural details of this bending between the hook and lever helices, and between the N- and C-lobes of the RLC. Because of its location at the junction between the two heads of each myosin molecule, the N-lobe of the RLC might also control the interactions between the two heads, and/or between the heads and the myosin filament backbone. Here, we determined the orientation of the N-lobe of the RLC in skeletal muscle fibers using BR probes attached to the A, B, C, and D helices of smRLC (Fig. 1). To test for possible differences between the orientation of smRLC and the native skRLC in skeletal muscle fibers,

Submitted October 29, 2011, and accepted for publication February 7, 2012.

*Correspondence: Malcolm.irving@kcl.ac.uk

David R. Trentham's present address is Randall Division of Cell and Molecular Biophysics, King's College London, London, United Kingdom.

Editor: Christopher Berger.

0006-3495/12/03/1418/9 $2.00

doi: 10.1016/j.bpj.2012.02.010

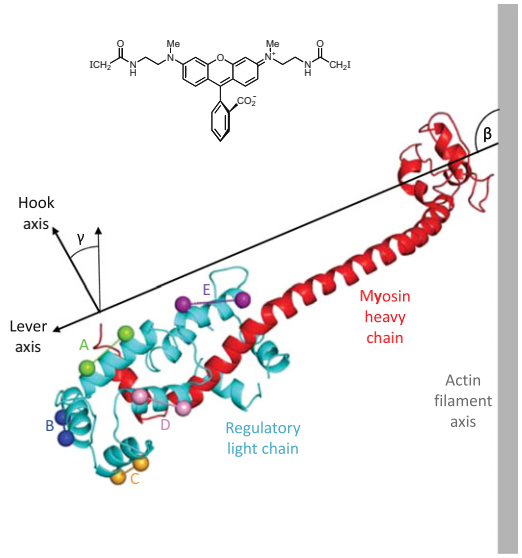

FIGURE 1 Location of bifunctional rhodamine (BR-I_2; *inset*) probes on the RLC. Residues 707–843 of the myosin heavy chain (*red*) with the bound RLC (*blue*) are shown in the orientation with respect to the actin filament axis (*gray*) seen in the nucleotide free (*rigor*) actin-myosin head complex (4,5). The ELC has been omitted for clarity. BR probes were introduced on the A (*green*), B (*dark blue*), C (*orange*), D (*pink*), and E (*purple*) helices of the RLC, cross-linking inserted cysteine residues denoted by each pair of spheres. The orientation of the LCD of the myosin head is described by the tilt (β) and twist (γ) angles defined in the text.

we repeated the measurements with a skeletal myosin RLC labeled on its D helix. To extend that test to the C-lobe where probes were placed for previous smRLC studies (14–16), we made similar experiments with skRLC labeled on its E helix (Fig. 1).

MATERIALS AND METHODS

Preparation and characterization of BR-smRLCs

Mutants of smRLC from chicken gizzard myosin with cysteines at positions 31 and 38 (CEFKEAFC) on helix A, 51 and 58 (CDLHDMLC) on helix B, 67 and 74 (CYLEGMMC) on helix C, and 83 and 91 (CMFLTMFGC) on helix D (Fig. 1), with Ala substituting for Cys at position 108 in each case were obtained by site-directed mutagenesis. Protocols were essentially as in (16) except that the pMW172 vector was used for protein expression (21,22). The masses in Daltons of the A, B, C, and D helix smRLC mutants were determined by electrospray mass spectrometry as 19,647 (cf. calculated mass 19,646), 19,690 (19,687), 19,671 (19,672), and 19,658 (19,658), respectively.

Each of the smRLC mutants was labeled with BR-I_2 and purified as described (16). These labeled RLCs are referred to as BR-smRLC-A, etc., where the last letter refers to the RLC helix where the BR probe is attached. Bifunctional labeling produces diastereoisomers, and these could be separated on a preparative scale for BR-smRLC-D. Other BR-smRLCs were studied as mixed diastereoisomers. Measured (calculated) masses (Daltons) of the BR-smRLC-A, BR-smRLC-B, BR-smRLC-C, and BR-smRLC-D were 20,175 (20,171), 20,214 (20,212), 20,196 (20,197), and 20,185 (20,183).

BR-smRLCs were purified and characterized by standard chromatography protocols monitored by absorption at 215 nm and fluorescence at 575 nm (14,16,23). The two diastereoisomers of BR-smRLC-D were well resolved by FPLC on a Mono-S HR cation exchange column (GE Healthcare, Chalfont, UK). The protein was eluted with a 150–300 mM KCl gradient in sterile filtered FPLC buffer (10 mM potassium phosphate, 50 mM potassium propionate, and 1 mM $MgCl_2$ at pH 7.0). Circular dichroism (CD) spectra of the resolved stereoisomers were measured in a JASCO J-715 spectropolarimeter. BR-smRLC function was assessed by calcium regulation of actomyosin ATPase activity of scallop myofibrils in which native RLCs had been replaced by BR-smRLCs, using reconstitution with native scallop RLC as a control (18–20).

Preparation and characterization of BR-skRLCs

Mutants of skRLC with cysteines at positions 78–86 (CVFLTMFGC) on helix D and 95–103 (CVIMGAFKC) on helix E (Fig. 1) with Ala substituted for Cys at positions 125 and 154 were obtained by site-directed mutagenesis and prepared as described in the Supporting Material. Electrospray mass spectrometry showed an extra Ala as a minority species in both skRLCs; measured mass in Daltons for skRLC-D was 18,551 (calculated mass 18,549) and +Ala 18,618 (18,620); for skRLC-E 18,572 (18,565), and +Ala 18,639 (18,636). Each skRLC mutant was labeled with BR-I_2 and purified as described (16). Mass spectrometry of mixed diastereoisomers showed the extra Ala in BR-skRLC-E as a minority species (measured mass 19,097 Daltons (calculated mass 19,090) and +Ala 19,163 (19,161)), but the corresponding extra Ala was not found in BR-skRLC-D (measured mass 19,075 (19,074)).

Muscle fiber experiments and interpretation of polarized fluorescence intensities

Fiber bundles were prepared from psoas muscles of New Zealand White rabbits as described previously, stored at –20°C, and used within 6 weeks (16). Segments of single muscle fibers 2–3 mm long were dissected from a bundle on the day of an experiment. Aluminum T-clips were crimped to the segment ends; one T-clip was attached to a force transducer and the other to a moveable hook (23). Sarcomere length was set to 2.4 μm. Each BR-RLC was separately incorporated into fibers in an EDTA exchange solution containing ~50 μM BR-RLC for 30 min at 30°C (23). Specific incorporation of BR-smRLCs into the A-bands of the muscle sarcomeres was confirmed by confocal microscopy (16). Whole troponin and troponin C were replaced in relaxing solution. Composition of storage, relaxing, RLC exchange, pre-activating, activating, and rigor solutions and activation protocols were as in (16). The experimental temperature was 10°C.

Fluorescence emission from the BR-RLC in a muscle fiber was collected by a 0.25 N.A. objective using excitation light beams either in line with or at 90° to the emission path (23). The polarization of the excitation and emitted beams were set either parallel or perpendicular to the fiber axis, allowing determination of the three-order parameters, $\langle P_{2d}\rangle$, $\langle P_2\rangle$, and $\langle P_4\rangle$ that describe the dipole orientation in the fiber (24). The orientation distribution of individual BR-RLCs with respect to the fiber axis was determined by one-dimensional maximum entropy (ME) analysis (25). The orientation of the N-lobe of the RLC was calculated by combining the data from the A, B, C, and D helix smRLC probes using two-dimensional ME analysis (15,26).

The orientation of each probe dipole in the coordinate frame of a given crystallographic structure was calculated with respect to the lever and hook axes in Fig. 1. For chicken skeletal myosin in the nucleotide-free state (2MYS; (4)) the lever axis joins the heavy chain α-carbons of Cys^{707} and Lys^{843}, and the hook axis joins the midpoints between the pairs Phe^{836}/Ile^{838} and Met^{832}/Leu^{834}. ϕ is the angle between the dipole and lever axes and ψ is the angle between the lever/dipole plane and the lever/hook plane. An increase in ψ denotes a counter-clockwise rotation of the dipole around the lever axis as viewed from Lys^{843}. The angular coordinates of the A, B, C, and D helix probes in this frame are: $\phi = 36.5°$, 118.6°, 98.3°, and

145.2°; $\psi = -75.1°$, $-132.5°$, 80.7°, and $-46.4°$, respectively. This analysis was extended to crystal structures of other myosin isoforms by selecting analogous residues to define the lever and hook axes in each isoform. In the case of the LCD structure of myosin from the catch muscle of the scallop *Placopecten magellanicus* (3PN7; (9)), the lever axis was defined by superimposition of the ELC region onto that of the nucleotide-free chicken skeletal myosin head (2MYS; (4)). These regions have a very similar fold, with a root mean-square deviation of 1.7 Å. Thus, molecule 1 of (9) has $\phi = 30.8°$, 122.2°, 101.0°, and 115.5°; $\psi = -69.9°$, $-117.2°$, 88.0°, and $-47.8°$ for the A, B, C, and D helix probes, and molecule 2 has $\phi = 52.8°$, 109.3°, 85.7°, and 153.2°; $\psi = -52.2°$, $-135.6°$, 80.6°, and $-67.6°$.

RESULTS

Double-cysteine mutants of RLC isoforms from chicken smooth or skeletal muscle (smRLC and skRLC) labeled with BR on the A, B, C, D, or E helix of the RLC (Fig. 1) were prepared, purified, and characterized as described in Materials and Methods. In general, because of the restricted rotation of the pendant phenyl group of the BR moiety with respect to the xanthene rings carrying the protein linkers (Fig. 1, *inset*), these BR-RLCs exist as a mixture of diastereoisomers. In some cases these could be separated chromatographically, and the separated diastereoisomers of smRLC labeled with BR on the D helix (BR-smRLC-D) exhibited CD spectra with mirror-image behavior (Fig. 2). Other BR-RLC diastereoisomers did not exhibit such clear mirror-image CD spectra.

The effect of mutagenesis and BR labeling on the smRLC function was assessed by exchanging them into scallop myofibrils, taking advantage of the ability of smRLC to replace the scallop RLC and thereby restore calcium regulation of the myofibrillar ATPase activity. In native scallop myofibrils, the ATPase rate was ~35 times higher in the presence of Ca^{2+} than in its absence (Table 1). Desensitized myofibrils, from which the scallop RLC had been extracted, had an ATPase control ratio of ~1, as did myofibrils into which skRLCs had been exchanged, as expected from previous results (19,20). The BR-smRLCs restored calcium regulation to the same extent as scallop RLC and unlabeled mutant smRLCs (Table 1). These results show that mutagenesis and BR labeling of the N-lobe helices of smRLC does not affect its ability to form a functional complex with the myosin heavy chain and ELC, in agreement with previous results for BR probes on the C-lobe of smRLC (14).

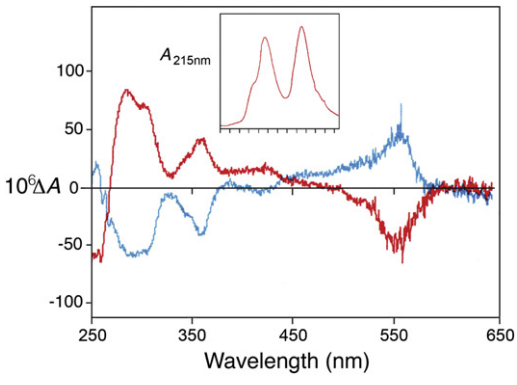

FIGURE 2 CD spectra of the diastereoisomers of the BR-smRLC-D. The CD spectra were measured in a 10 mm cell with an ordinate scale ΔA absorption parameter equal to $(A_L - A_R)$ where the subscripts define the polarization of the incident light. The inset shows the elution profile showing separation of the two diastereoisomers from a Mono-S column with an arbitrary absorption ordinate scale (zero relative to solvent at origin) and with individual fractions collected marked on the abscissa. The leading peak in the elution has the positive peak in its CD spectrum at 550 nm.

Orientation of the N-lobe of smRLC in skeletal muscle fibers; single probe data

The polarized fluorescence from BR probes attached to the A, B, C, or D helices of the N-lobe of smRLC was interpreted in terms of the order parameter $\langle P_{2d} \rangle$, which describes the amplitude of the independent motion of a probe with respect to the RLC on the subnanosecond timescale, and $\langle P_2 \rangle$ and $\langle P_4 \rangle$, which report the time-averaged orientation of a probe with respect to the actin filament or muscle fiber axis (24). $\langle P_{2d} \rangle$ was in the range 0.73–0.83 for all probes and conditions studied (Fig. 3), similar to values reported previously for BR probes on the C-lobe of smRLC in skeletal muscle fibers (16), and corresponding to subnanosecond wobble of the BR dipole in a cone of semiangle ~30°.

$\langle P_2 \rangle$ and $\langle P_4 \rangle$ are the second- and fourth-rank coefficients of the Legendre polynomial expansion of the distribution of angles θ between the probe dipole and the fiber axis. $\langle P_2 \rangle$ is +1 if $\theta = 0°$ and −0.5 if $\theta = 90°$. $\langle P_4 \rangle$ has a biphasic dependence on θ; it is +1 for $\theta = 0°$, −0.43 for $\theta = 50°$, and +0.375 for $\theta = 90°$. Increased orientational disorder is associated with order parameters closer to zero. The values of $\langle P_2 \rangle$ and $\langle P_4 \rangle$ measured for probes on the

TABLE 1 ATPase rates of scallop myofibrils containing different RLC isoforms

	$-Ca^{2+}(s^{-1})$	$+Ca^{2+}(s^{-1})$	$+Ca^{2+}/-Ca^{2+}$
Control myofibrils	0.03 ± 0.02	1.06 ± 0.54	35 ± 27
Desensitized myofibrils	0.57 ± 0.20	0.48 ± 0.18	0.8 ± 0.3
skRLC	0.42 ± 0.06	0.43 ± 0.10	1.0 ± 0.4
Scallop RLC	0.27 ± 0.20	1.09 ± 0.38	4.0 ± 1.3
BR-smRLC-A	0.19 ± 0.14	1.26 ± 0.35	6.6 ± 4.1 (3.4 ± 1.6)
BR-smRLC-B	0.54 ± 0.27	1.63 ± 0.60	3.0 ± 1.9 (4.8 ± 0.6)
BR-smRLC-D isomer 1	0.36 ± 0.09	1.23 ± 0.53	3.4 ± 0.9 (3.1 ± 2.0)
BR-smRLC-D isomer 2	0.21 ± 0.08	0.72 ± 0.22	3.4 ± 0.8 (3.3 ± 0.9)

Mean values (± SD) for $n = 6$ assays in each case from a single preparation. Data in brackets in the right column are for assays ($n = 4$ or 5 in each case from a single preparation) of the smRLC before labeling with BR-I_2.

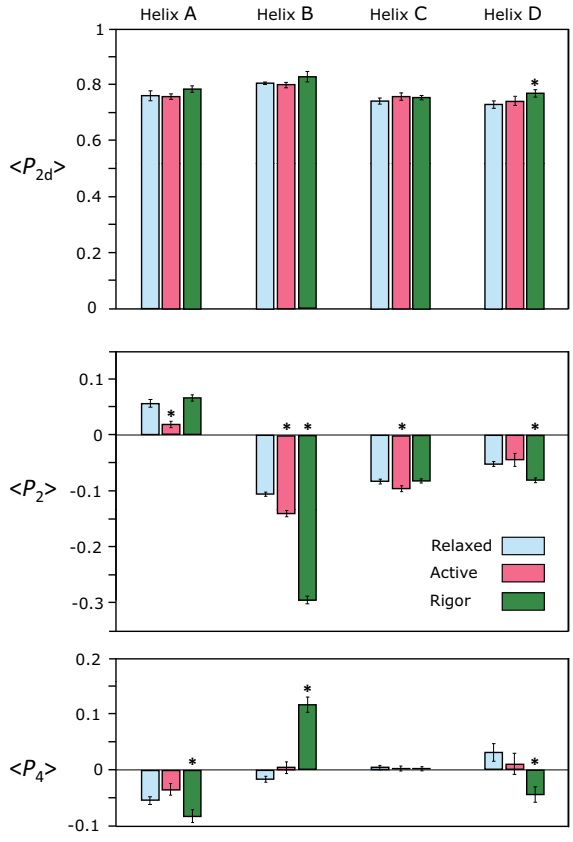

FIGURE 3 Order parameters $\langle P_{2d}\rangle$, $\langle P_2\rangle$, and $\langle P_4\rangle$ for the orientation of BR probes on the A, B, C, and D helices of smRLC in relaxed, active, and rigor states of permeabilized muscle fibers. Mean ± SE for 9 fibers, A-helix; 7 fibers, B-helix; 4–8 fibers, C-helix; and 10 fibers, D-helix. * denotes active and rigor values for which differences from relaxed are significant at the 5% level as determined by a *t*-test.

N-lobe of the RLC (Fig. 3) indicate substantial disorder in all conditions studied, with less disorder in rigor than in relaxation or isometric contraction, again as observed previously for probes on the C-lobe (16). The order parameters were reproducibly different in the three fiber states, notably for the B helix, which becomes considerably more perpendicular to the fiber axis in rigor. There was no significant difference between the measured order parameters for the two diastereoisomers of BR-smRLC-D, and these data have been combined in Fig. 3.

Comparison of orientations of probes on smooth and skeletal muscle RLCs

The orientation data for the N-lobe of the RLC in skeletal muscle fibers described above (Fig. 3) were obtained using bifunctional probes attached to smRLC, as in earlier studies of the C-lobe (14–16). We repeated the experiments using a skRLC with the BR probe on its D helix. The order parameters measured with BR-skRLC-D were similar but not identical to those measured with BR-smRLC-D. For example, in rigor, $\langle P_2\rangle$ was -0.048 ± 0.003 ($n = 5$) for BR-skRLC-D and -0.078 ± 0.004 ($n = 10$) for BR-smRLC-D; the corresponding values for $\langle P_4\rangle$ were -0.067 ± 0.004 and -0.044 ± 0.010, respectively.

The angular changes represented by these differences were estimated by calculating the smoothest distribution of angles between the probe dipole and the fiber axis consistent with each set of $\langle P_2\rangle$ and $\langle P_4\rangle$ values. This one-dimensional maximum entropy (ME) distribution (25) was then represented by its mean (θ_{ME}) and standard deviation (σ_{ME}). θ_{ME} and σ_{ME} were similar, within a few degrees, for the BR-skRLC-D and BR-smRLC-D data in all conditions studied (Table 2). We conclude that the D helices of smRLC and skRLC have almost the same orientation after exchange into a skeletal muscle fiber, although the possibility remains that the N-lobe has a different rotation around the D helix for the two isoforms.

Because the previous studies of the orientation of the C-lobe of RLC (14–16) also used BR-smRLCs, we measured polarized fluorescence from fibers containing a skRLC labeled with BR on its E helix, in the C-lobe. θ_{ME} and σ_{ME} for BR-skRLC-E were again within a few degrees of the values for BR-smRLC-E in all conditions studied (Table 2). The largest difference was in rigor, with the E helix of the skeletal RLC isoform ~4° more perpendicular to the fiber axis. Thus, as in the case of the N-lobes, these results suggest that the C-lobes of smRLC and skRLC have similar but not identical orientations in skeletal muscle fibers. The smRLC data were used for the analysis described below.

Orientation of the N-lobe of smRLC in skeletal muscle fibers; multiple probe analysis

The orientation of the N-lobe of the RLC in skeletal muscle fibers was determined from the order parameters measured

TABLE 2 Orientation of BR probes on the D and E helices of smRLC and skRLC

	Relaxed		Active		Rigor	
	θ_{ME}	σ_{ME}	θ_{ME}	σ_{ME}	θ_{ME}	σ_{ME}
smRLC-D	59.6 ± 0.2	22.0 ± 0.4	59.0 ± 0.5	21.4 ± 0.6	60.6 ± 0.2	18.9 ± 0.3
skRLC-D	57.0 ± 0.1*	20.9 ± 0.1†	56.6 ± 0.2*	20.9 ± 0.1†	59.0 ± 0.1*	18.8 ± 0.2†
smRLC-E	59.4 ± 0.2	19.6 ± 0.2	57.9 ± 0.1	20.5 ± 0.4	62.3 ± 0.3	18.0 ± 0.3
skRLC-E	59.0 ± 0.2†	22.1 ± 0.2*	57.1 ± 0.2*	22.9 ± 0.2*	66.6 ± 0.6*	18.8 ± 0.4†

θ_{ME} and σ_{ME} are the mean and standard deviation of a one-dimensional ME distribution calculated from the $\langle P_2\rangle$ and $\langle P_4\rangle$ values for each probe. Data are means (± SE) in degrees for; 10 fibers, BR-smRLC-D; 4–5 fibers, BR-skRLC-D; 7 fibers, BR-smRLC-E; and 4 fibers, BR-skRLC-E. Statistical significance of differences between values for skRLC and smRLC was assessed using the *t*-test: *$P < 0.05$; $^{\dagger}P > 0.05$.

from probes on its A, B, C, and D helices using a crystallographic structure of the RLC region of the myosin head to constrain the three-dimensional angles between the helices, following the approach used previously for the C-lobe (14–16). Initially, we used the nucleotide-free structure of the head domain of chicken skeletal myosin (2MYS; (4)) to calculate the inter-probe angles, under the assumption that each probe dipole is parallel to the line joining the β-carbons of the cysteines to which it is attached (27). The consequences of using other crystallographic structures of the RLC region are considered in the Discussion section.

As in the previous C-lobe studies, we define a coordinate frame in the myosin head in terms of a lever axis, linking residues 707 and 843 of the myosin heavy chain ((4); Fig. 1), and a hook axis, parallel to the short hook helix at the C-terminus of the heavy chain in the head (15,16). The orientation of each probe in the protein frame was described in terms of ϕ, the angle between the dipole and the lever axis, and ψ, the angle between the lever/dipole plane and the lever/hook plane (see Methods for details). The orientation of the RLC region in a muscle fiber was expressed as β, the tilt angle between the lever axis and the actin filament, and γ, describing rotation of the RLC region around the lever axis, when $\gamma = 0$ the hook axis is in the same plane as the lever and filament axes (Fig. 1).

We used a ME formalism (26) to calculate the smoothest distribution of (β, γ) orientations consistent with the measured $\langle P_2 \rangle$ and $\langle P_4 \rangle$ values from probes on the A, B, C, and D helices of the RLC. These ME distributions accurately represent the major features of the (β, γ) distribution, but may not reveal local deviations from a smooth distribution or small populations of probes with different orientations (26). The ME distributions of the orientation of the RLC regions of myosin heads in a muscle fiber calculated from probes on the A, B, C, and D helices of smRLC were represented by two-dimensional contour plots of β and γ, with hotter colors representing more common (β, γ) orientations (Fig. 4). The most common or peak (β, γ) orientation of the RLC region is approximately the same in relaxation, isometric contraction, and rigor conditions (Fig. 4, *A*, *B*, and *C*, respectively), with β within the range 100–110° and γ ~40°. The orientation distribution is narrower in rigor. In general, the polarized fluorescence technique used here cannot distinguish between the orientations (β, γ) and ($180° - \beta$, $180° + \gamma$), a transformation that corresponds to the two ends of a dipole probe or to RLC molecules in the two halves of each muscle sarcomere. However, for the RLC regions of myosin heads that are attached to actin, this ambiguity can be resolved by applying rapid changes of fiber length (14,15), showing that the solution with $-90° < \gamma < 90°$, the region plotted in Fig. 4, applies to actin-attached myosin heads. For this solution the C-terminus of the hook helix at the myosin head/rod junction points toward the M line of the sarcomere, consistent with its role in bearing axial force. β then takes a specific meaning at the level of the muscle half-sarcomere: an increase in β means that actin-attached myosin heads tilt in the same direction as during muscle shortening. The peak β in rigor, close to 100°, is similar to that in the RLC region of isolated myosin heads bound to actin filaments in rigor determined by fitting the crystal structure of the nucleotide-free chicken skeletal myosin head into electron micrographs of the complex, 102° (4,5) and 108° (28). The peak γ determined here, ~40° in rigor, is larger than that determined in those in vitro studies (−2° and 8°, respectively).

The (β, γ) orientation distributions calculated from the four probes on the N-lobe of the RLC suggest that there is a minor population of heads with $\beta = 80°$, $\gamma = -40°$ in relaxing conditions (Fig. 4 *A*), a region in which a tail is also seen in the ME distribution calculated from the C-lobe probes (16). In isometric contraction the N-lobe distribution indicates a minor population of probes around $\beta = 60°$, $\gamma = +40°$ (Fig. 4 *B*), but this is much less prominent than the density seen around $\beta = 70°$ in ME distributions determined using C-lobe probes (15), which also extends broadly across the $\gamma = 0°$ axis. The diagonal stretching of the peak of the ME distribution in rigor (Fig. 4 *C*), with a positive correlation between β and γ, was also observed with the C-lobe probes (15,16).

DISCUSSION

We used a set of four myosin RLCs labeled with the BR probe on different helices of its N-terminal lobe to determine the orientation of this region of the myosin heads in

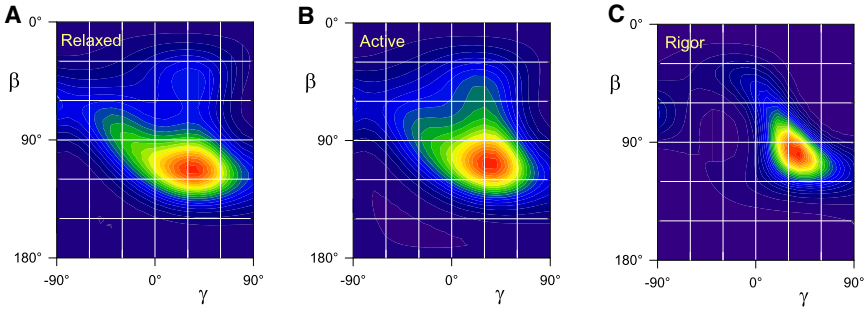

FIGURE 4 ME distributions of the orientation of the LCD of the myosin heads in relaxation (*A*), active isometric contraction (*B*), and rigor (*C*). Tilt (β) and twist (γ) angles are shown in Fig. 1 and defined in the text. Orientation distributions calculated from the order parameters in Fig. 3 using the nucleotide-free structure of the chicken skeletal myosin head (4), and normalized to peak intensity. Hotter colors denote a greater probability of that (β, γ) orientation.

skeletal muscle fibers in relaxation, isometric contraction, and rigor. The peak orientation in all three states has the lever axis of the heads at an angle (β) of 100–110° to the actin filament axis, and the C-terminal hook helix rotated out of the lever/filament plane by an angle (γ) of ~40°. The orientation distribution is sharper in rigor than in relaxation or isometric contraction, but all three states show evidence of orientational heterogeneity. This may be related to the presence of two heads in each myosin molecule, the heterogeneity of biochemical and mechanical states of the heads, the mismatch between the axial periodicities of the heads and their actin-binding sites, and the involvement of tilting of the LCD in the elastic distortion of the heads.

The in situ orientation of the RLC region determined here using BR probes on its N-lobe (Fig. 4) is broadly similar to that determined previously from probes on the C-lobe (14–16) and on the ELC (17), but there are some quantitative differences. For example, the peak (β, γ) orientation in rigor was 100°, 40° from the N-lobe probes, compared with 80°, 22° (15) or 85°, 25° (16) from C-lobe RLC probes, and 120°, 25° from probes on the ELC (17). The differences observed in relaxation and isometric contraction are more subtle and relate to the shape of the distributions as well as to the peak orientation. The peak (β, γ) in relaxing conditions also depends on temperature; it was 110°, 35° for the N-lobe probes at 10°C, compared with 100°, 0° for the C-lobe probes at 5°C, and 110°, 20° at 20°C (16). The ME distributions calculated from ELC probes in relaxing conditions at 10°C indicated the presence of two probe populations, both with peak β around 105–110° but with a γ peak at about $-50°$ as well as at $+20°$ (17). All these comparisons are presented for the $-90° < \gamma < 90°$ solution for consistency with Fig. 4. The differences between the orientations of the light-chain region of the myosin heads calculated from the N- and C-lobe RLC probe data suggest that the relative orientation of the two lobes in a muscle fiber is different from that in the crystal structure used to interpret the probe data. The difference in peak β in rigor, 100° from the N-lobe probes and 80° from the C-lobe probes, corresponds to movement of the C-terminus of an actin-attached myosin head by ~3.5 nm along the filament with respect to its attachment site. Because the motion produced by such bending represents a significant fraction of the 6–11-nm working stroke in the myosin head (13), it could be functionally important.

The conclusion that the conformation of the RLC region of the myosin head in a muscle fiber is different from that in crystals of nucleotide-free chicken skeletal myosin (2MYS; (4)) seems unlikely to be due to a limitation or artifact of the experimental approach used here. Results from a wide range of techniques provide evidence that replacement of the native RLC in a muscle fiber by BR-labeled RLCs preserves fiber function and RLC structure. The RLC exchange protocol used here, involving a 30 min incubation in low [Mg^{2+}] rigor solution at 30°C, results in replacement of 60–70% of the native RLCs by BR-RLC (16,29). As in the previous studies (16,29), confocal microscopy showed that the BR-RLCs were incorporated specifically into the myosin-containing A-bands of the sarcomere. Isometric force is slightly lower after RLC exchange, using either smRLC labeled with BR on its C-lobe (16,29), or skRLC labeled with iodoacetamidotetramethylrhodamine on either the N- or C-lobe (30), but this appears to be a nonspecific effect of the RLC exchange protocol rather than an effect of RLC isoform or the presence of the BR label per se (16,29).

RLC structure and function was also assessed in this work using the scallop myofibril ATPase regulation assay, taking advantage of the fact that smRLC can replace the native scallop RLC to restore Ca^{2+} regulation in this system (19,20). smRLCs both unlabeled and labeled with BR on the N-lobe also restored Ca^{2+} regulation in this assay, as shown previously for smRLCs labeled on the C-lobe (14). Because Ca^{2+} regulation in this system depends on the precise fold of the RLC, and can be abolished by mutagenesis of a single residue at the RLC/ELC interface (31), these results provide strong evidence that BR attachment and RLC exchange do not affect the native fold of the RLC. skRLCs do not support Ca^{2+} regulation in the scallop myofibril assay, but the comparison of polarized fluorescence data for smRLC and skRLC (Table 2) suggests that these two isoforms take up similar conformations within a skeletal muscle fiber, at least within a few degrees, so it seems likely that the above conclusion can be extended to skRLC. In addition, NMR studies of troponin C with BR attached as in this work to a pair of surface-accessible cysteines in a α-helix, showed that BR attachment does not affect the backbone fold of the protein (32).

There is one known limitation of the conclusion that replacement of the native RLC in a skeletal muscle fiber by BR-RLCs does not affect RLC structure or function. X-ray diffraction patterns from bundles of rabbit psoas fibers in relaxing solution at 20°C showed a decrease in the intensity of the myosin-based axial and layer-line reflections following a smRLC exchange protocol like that used here, suggesting that the axial and helical order of the myosin heads on the surface of the thick filaments had been reduced (29). These results suggest that the helically ordered structure of the thick filaments seen in mammalian muscle at 20°C (33) is disrupted by incorporation of BR-smRLC, leaving the more disordered structure normally seen at lower temperature.

Two further general questions might be raised about the assumptions made in our interpretation of the probe data, namely that the probe dipole is parallel to the line joining the two cysteines to which it is attached, and that the conformation of the RLC is the same as in the crystal structure used to interpret the polarized fluorescence data. Both assumptions relate to the values of the angles ϕ and ψ that are used in the analysis (see Materials and Methods) to

describe the orientation of a probe dipole in the coordinate frame of the RLC.

The assumption about the relative orientation of the probe dipole and the line joining its cysteine attachment points has been addressed by molecular dynamics for the example of BR attached to a surface helix of troponin C from skeletal muscle (27). The results showed that the flexible linkers between the xanthene fluorophore and the attachment points on the helix allow independent motion of the probe dipole with respect to the protein. In addition to subnanosecond wobble of the probe that contributes to $\langle P_{2d} \rangle$, hydrophobic interactions between the xanthene ring system and the protein surface can introduce an offset between the time-averaged orientation of the probe dipole and the line joining its attachment points, i.e., an uncertainty in ϕ and ψ, of the order of 10°.

The possibility of a difference between ϕ and ψ in the muscle fiber and in the crystal structure used to interpret the fluorescence data is more fundamental, and has general implications for the extrapolation from crystallographic structures to in situ structures. The values of ϕ and ψ differ widely between published crystallographic structures of the RLC region of the myosin head (4,7,9,34,35). For example, ϕ and ψ for the D helix RLC probe are 145.2 and −46.4° in nucleotide-free chicken skeletal myosin (2MYS; (4)) but 162.5 and −98.8° for a nucleotide-free myosin from scallop striated muscle (1SR6; (34)). Thus, the differences between ϕ and ψ values for different crystal structures can be much larger than the ~10° uncertainty related to independent motion of the probe with respect to its protein attachments. Moreover, these relatively large differences between crystallographic ϕ and ψ values are not simply due to differences in bound nucleotide or myosin isoform, as most clearly demonstrated by a recent x-ray study of the LCD of a myosin from the catch muscle of the scallop *Placopecten magellanicus* (9). The crystallographic unit cell in that study contained two molecules with different bends between the N- and C-lobes of the RLC, indicating a point of flexibility within the RLC region. The pivot point was within the RLC D helix, at a conserved glycine (residue 85 in chicken skeletal RLC) near its C-terminus, suggesting that bending at this point in the RLC is a generic property of muscle myosins. Moreover, within the N-lobe, the angle between the A and D helices differed by ~40° between the two molecules; the bend is associated with a different conformation of the N-lobe.

To investigate the effect of these different RLC conformations on the interpretation of the present results, we used the two structures of the RLC region of scallop catch muscle myosin (9) to calculate ME distributions of LCD from the order parameters reported here for the four probes on its N-lobe (see Materials and Methods for details). These ME distributions (Fig. 5) retain key features of the maps calculated using the coordinates of chicken skeletal myosin (Fig. 4), in particular the similar orientation of the main peak in relaxation, isometric contraction and rigor, and the narrower peak in rigor. There are also some striking differences. The molecule 1 distributions (Fig. 5, *A–C*), have peak β 100–110°, like those obtained using coordinates from chicken skeletal myosin (2MYS; (4); Fig. 4), but more prominent tails at lower β and γ, most obviously in rigor (Fig. 5 *C*). The molecule 2 distributions (Fig. 5, *D–F*), have a lower peak β in general. The rigor peak (Fig. 5 *F*) is relatively narrow at around β, $\gamma = 80°$, 35°, but in

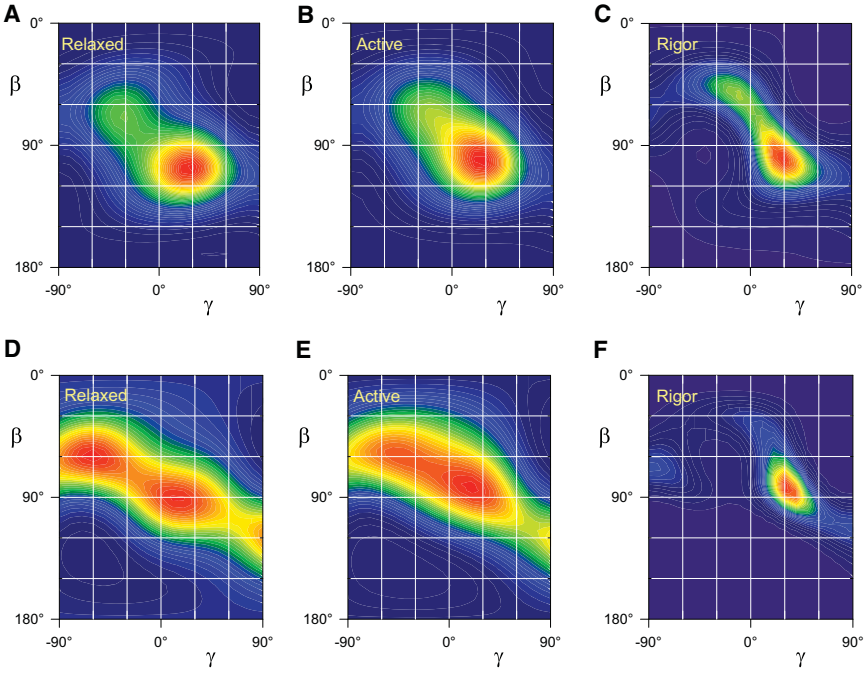

FIGURE 5 ME distributions of the orientation of the LCD of the myosin heads in relaxation (*A* and *D*), active isometric contraction (*B* and *E*) and rigor (*C* and *F*). Orientation distributions calculated from the order parameters in Fig. 3 using the molecule 1 (*A–C*) and molecule 2 (*D–F*) structures of the LCD of myosin from scallop catch muscle (9).

relaxation (Fig. 5 *D*) there are two broad peaks of almost equal amplitude, centered around β, $\gamma = 60°$, $-60°$ and 90°, 20°, but with a large dispersion in γ for both peaks. In isometric contraction (Fig. 5 *E*) these two peaks are less clearly separated.

When a similar analysis was carried out using published $\langle P_2 \rangle$ and $\langle P_4 \rangle$ data from four probes on the C-lobe of the RLC in relaxing and rigor conditions (16), the ME maps calculated from the molecule 1 and 2 structures had the same shape and the same peak β, but the peak γ was ~35° larger for the molecule 2 map (Fig. S1). This result is expected from the similar conformation of the RLC C-lobes in the two molecules combined with the different twist between the N- and C-lobes that rotates the hook axis by ~35° with respect to the C-lobe, leading directly to the 35° difference in γ in the ME maps in Fig. S1.

The bend between the N- and C-lobes of the RLC in a muscle fiber is within the range of bends in published crystal structures. The crystal structure that most closely matched the bend in the RLC in a rigor muscle fiber, as determined by the comparative N-lobe/C-lobe analysis described above, was that of squid myosin in the rigor-like state (2OVK, (35); Fig. S2). The peak of the β, γ ME distribution in rigor muscle fibers calculated using the 2OVK coordinates was 90°, 20° for the N-lobe and 90°, 10° for the C-lobe (Fig. S2); we consider these to be equal within the precision of the present technique. The corresponding values for relaxed muscle fibers, for which the ME analysis showed a single peak for both lobes, were 100°, 10° and 90°, −20°, respectively, and here the difference in γ is probably significant. This example, together with the ME analyses using the original nucleotide-free crystal structure of chicken skeletal myosin (Fig. 4) and the two crystal structures of myosin from scallop catch muscle, suggests that the bend between the N- and the C-lobes of the RLC depends on the state of the muscle fiber, and may therefore be functionally significant. In relaxed and actively contracting fibers the myosin heads in different nucleotide or in actin-attached or detached states may have different RLC conformations. In general, the possible coexistence of multiple RLC conformations in a muscle fiber, some of which have different inter-helix angles within the N-lobe (e.g., between the A and D helices), means that the data from the four BR-RLC probes used here cannot be used to determine which or if any of the crystallographic conformations is taken up in a muscle fiber in a given state. However, the orientation of the N-lobe of the RLC in rigor fibers was relatively insensitive to the choice of crystallographic model; the peak β, γ was between 80°, 20° and 100°, 35° in all cases.

Bending between the N- and C-lobe of the RLC, like that between the RLC and the ELC (7,17) and between the motor domain and the ELC (8), seems at first sight inconsistent with the usual assumption in lever arm models of the myosin motor mechanism that the LCD is a rigid lever arm. However, in the intact sarcomere the bending range may be limited by steric clash with other regions of the heads, the other head of each myosin molecule, or the filament backbone. In a force-bearing myosin head, the bend may already be at one end of the sterically accessible range and thus not contribute further to head compliance or the working stroke. These internal bends in the light chain region might rather be involved in controlling the interaction between the two heads of each myosin molecule in relaxing conditions, as in smooth muscle and invertebrate skeletal muscle. These hypotheses remain to be tested by future work.

Finally, these considerations might be extended to bending between the LCD of the myosin head and the adjacent coiled-coil rod region of the myosin heavy chain that joins it to the myosin filament backbone, at residue 843 of the heavy chain in skeletal muscle myosin. Molecular models of the mechanism of muscle contraction generally assume free rotation about the head-rod junction, although again it seems likely that intermolecular interactions might constrain such rotation in the intact sarcomere. The present observation that the orientation of the N-lobe of the RLC, immediately adjacent to residue 843, is similar in relaxed, contracting, and rigor muscle might be more readily explained by steric restriction of the interaction between the N-lobe and the filament backbone, although other explanations cannot presently be excluded.

SUMMARY

We have measured the orientation of the N-lobe of the myosin RLC in skeletal muscle fibers, and shown that the peak orientation of the N-lobe is similar in relaxation, isometric contraction, and rigor. The relative orientation between the N- and C-lobes of the RLC in fibers is intermediate between those in published crystal structures of this region of myosin, suggesting that bending between these two lobes occurs in situ, and may have general functional significance in the contraction and regulation of skeletal muscle.

SUPPORTING MATERIAL

Materials and methods and two figures are available at http://www.biophysj.org/biophysj/supplemental/S0006-3495(12)00210-X.

We are grateful to Roisean E. Ferguson (Cancer Research UK Clinical Centre, St. James University Hospital, Leeds, UK), Andrew S. Brack (Massachusetts General Hospital, Center of Regenerative Medicine, Harvard University, Boston, MA), Stephen R. Martin (Medical Research Council (MRC) National Institute for Medical Research, Mill Hill, London, UK), and Robert E. Dale, John E. T. Corrie, Sophia Tincey, and John Kendrick-Jones (MRC Laboratory of Molecular Biology, Hills Road, Cambridge, UK) for help and advice.

We are also grateful to the MRC (UK) and Biotechnology and Biological Sciences Research Council (UK) for financial support.

REFERENCES

1. Huxley, H. E. 1969. The mechanism of muscular contraction. *Science.* 164:1356–1365.
2. Lymn, R. W., and E. W. Taylor. 1971. Mechanism of adenosine triphosphate hydrolysis by actomyosin. *Biochemistry.* 10:4617–4624.
3. Huxley, A. F., and R. M. Simmons. 1971. Proposed mechanism of force generation in striated muscle. *Nature.* 233:533–538.
4. Rayment, I., W. R. Rypniewski, …, H. M. Holden. 1993. Three-dimensional structure of myosin subfragment-1: a molecular motor. *Science.* 261:50–58.
5. Rayment, I., H. M. Holden, …, R. A. Milligan. 1993. Structure of the actin-myosin complex and its implications for muscle contraction. *Science.* 261:58–65.
6. Geeves, M. A., and K. C. Holmes. 1999. Structural mechanism of muscle contraction. *Annu. Rev. Biochem.* 68:687–728.
7. Houdusse, A., and C. Cohen. 1996. Structure of the regulatory domain of scallop myosin at 2 Å resolution: implications for regulation. *Structure.* 4:21–32.
8. Houdusse, A., A. G. Szent-Gyorgyi, and C. Cohen. 2000. Three conformational states of scallop myosin S1. *Proc. Natl. Acad. Sci. USA.* 97:11238–11243.
9. Brown, J. H., V. S. Kumar, …, C. Cohen. 2011. Visualizing key hinges and a potential major source of compliance in the lever arm of myosin. *Proc. Natl. Acad. Sci. USA.* 108:114–119.
10. Pylypenko, O., and A. M. Houdusse. 2011. Essential "ankle" in the myosin lever arm. *Proc. Natl. Acad. Sci. USA.* 108:5–6.
11. Wendt, T., D. Taylor, …, K. Taylor. 2001. Three-dimensional image reconstruction of dephosphorylated smooth muscle heavy meromyosin reveals asymmetry in the interaction between myosin heads and placement of subfragment 2. *Proc. Natl. Acad. Sci. USA.* 98:4361–4366.
12. Irving, M., T. St Claire Allen, …, Y. E. Goldman. 1995. Tilting of the light-chain region of myosin during step length changes and active force generation in skeletal muscle. *Nature.* 375:688–691.
13. Piazzesi, G., M. Reconditi, …, V. Lombardi. 2007. Skeletal muscle performance determined by modulation of number of myosin motors rather than motor force or stroke size. *Cell.* 131:784–795.
14. Corrie, J. E. T., B. D. Brandmeier, …, M. Irving. 1999. Dynamic measurement of myosin light-chain-domain tilt and twist in muscle contraction. *Nature.* 400:425–430.
15. Hopkins, S. C., C. Sabido-David, …, Y. E. Goldman. 2002. Orientation changes of the myosin light chain domain during filament sliding in active and rigor muscle. *J. Mol. Biol.* 318:1275–1291.
16. Brack, A. S., B. D. Brandmeier, …, M. Irving. 2004. Bifunctional rhodamine probes of Myosin regulatory light chain orientation in relaxed skeletal muscle fibers. *Biophys. J.* 86:2329–2341.
17. Knowles, A. C., R. E. Ferguson, …, M. Irving. 2008. Orientation of the essential light chain region of myosin in relaxed, active, and rigor muscle. *Biophys. J.* 95:3882–3891.
18. Chantler, P. D., and A. G. Szent-Györgyi. 1980. Regulatory light-chains and scallop myosin. Full dissociation, reversibility and co-operative effects. *J. Mol. Biol.* 138:473–492.
19. Sellers, J. R., P. D. Chantler, and A. G. Szent-Györgyi. 1980. Hybrid formation between scallop myofibrils and foreign regulatory light-chains. *J. Mol. Biol.* 144:223–245.
20. Rowe, T., and J. Kendrick-Jones. 1992. Chimeric myosin regulatory light chains identify the subdomain responsible for regulatory function. *EMBO J.* 11:4715–4722.
21. Reinach, F. C., K. Nagai, and J. Kendrick-Jones. 1986. Site-directed mutagenesis of the regulatory light-chain Ca^{2+}/Mg^{2+} binding site and its role in hybrid myosins. *Nature.* 322:80–83.
22. Way, M., B. Pope, …, A. G. Weeds. 1990. Identification of a region in segment 1 of gelsolin critical for actin binding. *EMBO J.* 9:4103–4109.
23. Sabido-David, C., B. Brandmeier, …, M. Irving. 1998. Steady-state fluorescence polarization studies of the orientation of myosin regulatory light chains in single skeletal muscle fibers using pure isomers of iodoacetamidotetramethylrhodamine. *Biophys. J.* 74:3083–3092.
24. Dale, R. E., S. C. Hopkins, …, Y. E. Goldman. 1999. Model-independent analysis of the orientation of fluorescent probes with restricted mobility in muscle fibers. *Biophys. J.* 76:1606–1618.
25. Julien, O., Y.-B. Sun, …, M. Irving. 2007. Toward protein structure in situ: comparison of two bifunctional rhodamine adducts of troponin C. *Biophys. J.* 93:1008–1020.
26. van der Heide, U. A., S. C. Hopkins, and Y. E. Goldman. 2000. A maximum entropy analysis of protein orientations using fluorescence polarization data from multiple probes. *Biophys. J.* 78:2138–2150.
27. De Simone, A., J. E. T. Corrie, …, F. Fraternali. 2008. Conformation and dynamics of a rhodamine probe attached at two sites on a protein: implications for molecular structure determination in situ. *J. Am. Chem. Soc.* 130:17120–17128.
28. Holmes, K. C., I. Angert, …, R. R. Schröder. 2003. Electron cryomicroscopy shows how strong binding of myosin to actin releases nucleotide. *Nature.* 425:423–427.
29. Ling, N., C. Shrimpton, …, M. Irving. 1996. Fluorescent probes of the orientation of myosin regulatory light chains in relaxed, rigor, and contracting muscle. *Biophys. J.* 70:1836–1846.
30. Sabido-David, C., S. C. Hopkins, …, M. Irving. 1998. Orientation changes of fluorescent probes at five sites on the myosin regulatory light chain during contraction of single skeletal muscle fibres. *J. Mol. Biol.* 279:387–402.
31. Jancso, A., and A. G. Szent-Györgyi. 1994. Regulation of scallop myosin by the regulatory light chain depends on a single glycine residue. *Proc. Natl. Acad. Sci. USA.* 91:8762–8766.
32. Mercier, P., R. E. Ferguson, …, B. D. Sykes. 2003. NMR structure of a bifunctional rhodamine labeled N-domain of troponin C complexed with the regulatory "switch" peptide from troponin I: implications for in situ fluorescence studies in muscle fibers. *Biochemistry.* 42:4333–4348.
33. Lowy, J., D. Popp, and A. A. Stewart. 1991. X-ray studies of order-disorder transitions in the myosin heads of skinned rabbit psoas muscles. *Biophys. J.* 60:812–824.
34. Risal, D., S. Gourinath, …, C. Cohen. 2004. Myosin subfragment 1 structures reveal a partially bound nucleotide and a complex salt bridge that helps couple nucleotide and actin binding. *Proc. Natl. Acad. Sci. USA.* 101:8930–8935.
35. Yang, Y., S. Gourinath, …, C. Cohen. 2007. Rigor-like structures from muscle myosins reveal key mechanical elements in the transduction pathways of this allosteric motor. *Structure.* 15:553–564.